Fuel Processing Technology 199 (2020) 106302

Contents lists available at ScienceDirect

Fuel Processing Technology

journal homepage: www.elsevier.com/locate/fuproc

Activity and selectivity of methanol-to-olefin conversion over Zr-modified H-SAPO-34/H-ZSM-5 zeolites - A theoretical study

Duichun Li[a], Bin Xing[a], Baojun Wang[b,*], Ruifeng Li[a,*]

[a] College of Chemistry and Chemical Engineering, Taiyuan University of Technology, Taiyuan, Shanxi 030024, China
[b] Key Laboratory of Coal Science and Technology of Ministry of Education and Shanxi Province, Taiyuan University of Technology, Taiyuan, Shanxi 030024, China

ARTICLE INFO

Keywords:
Density functional theory
Methanol-to-olefins conversion
Frameworks structure
Acid strength
Activity and selectivity

ABSTRACT

The effect of Zr on the framework structure and acid strength of doped H-SAPO-34 and H-ZSM-5 was studied using the density functional theory considering dispersive interactions (DFT-D2). The activity and selectivity in methanol-to-olefins (MTO; in this work, olefins refer to ethylene and propylene) conversion over Zr doped H-SAPO-34 and H-ZSM-5 were systematically evaluated as a function of frameworks' structure and acid strength. The results were compared with those of their non-doped counterparts. The results indicated that doping of Zr into H-SAPO-34 exhibited larger pore volume, whereas the doping of Zr into H-ZSM-5 had little effect on pore volume. The acid strengths of both the Zr doped were reduced. It was found that doping of Zr into H-SAPO-34 led to enhanced activity, whereas doping of Zr into H-ZSM-5 had either little or no effect on activity. It can be concluded that the steric constraints, exerted by the larger cavity, are favorable for the MTO conversion. Both Zr doped H-SAPO-34 and H-ZSM-5 exhibited relatively higher ethylene selectivity. The acid strength of is closely related to the product selectivity during MTO conversion. The catalysts with weaker acid strengths displayed a higher selectivity towards ethylene.

1. Introduction

The conversion of methanol to olefins (MTO) over acidic zeolite catalysts is a nonpetroleum route to obtain light olefins (such as, ethylene and propylene) and has attracted considerable attention in recent years. It is well known that methanol can be easily produced using syngas from coal, natural gas, and biomass [1,2]. During the past decades, a great deal of effort has been devoted to elucidating the reaction mechanism of MTO using both the experimental and theoretical investigations [3–10]. It is widely accepted that MTO conversion proceeds through the hydrocarbon pool (HCP) mechanism proposed by Dahl and Kolboe, which describes that certain organic molecules, known as the HCP species, are trapped in the pores of zeolites and interplay with the Brönsted acid sites of the inorganic framework. These organic molecules serve as a cocatalyst. The alkyl chain is formed through continuous methylations and the olefins products are eliminated from the HCP in a closed catalytic cycle [8,9]. According to the type of HCP species, the HCP mechanism can be further divided into aromatic-based and alkene-based cycles [2,11]. Wang et al. utilized the kinetic Monte Carlo simulation and reported that the alkene-based cycles, especially the branched olefins, are more favorable than the aromatic-based cycles [12]. Therefore, the alkene-based cycles, in which higher olefins, such as 2, 3-dimethyl-2-butene (iso-C6) serve as the active HCP species [13], are based on the repeated methylation and cracking of alkenes, and therefore, are adopted as the mechanism of MTO conversion in this work.

A variety of acidic zeolites have been employed as the catalysts for MTO conversion [2,3,10,13–16]. Among all zeolites different topologies, H-SAPO-34 and H-ZSM-5 have proven to be the most promising for the MTO conversion, and are characterized by their relatively high activity and distinct selectivity towards light olefins [15]. H-SAPO-34 presented high selectivity for light olefins, such as ethylene and propylene [17]. The selectivity for ethylene and propylene over H-ZSM-5 is slightly inferior due to strong acidity, and a large number of aromatics were detected. [17–19]. Nevertheless, improving the selectivity of a single pathway towards a single species, especially ethylene, remains a challenge for researchers. In the MTO process, different topological structures and a variation in acidity are the two key factors controlling the catalytic activity and product selectivity of these materials [18,20–22]. With respect to the topological structure, the H-SAPO-34 has the chabazite (CHA) structure that features large cages connected through 8-member ring openings, whereas the H-ZSM-5 has the MFI structure, featuring crossed 10-member ring channels, and a particular interconnected channel system [23] compared to the 8-member ring in

* Corresponding author.
E-mail addresses: xingbin@tyut.edu.cn (B. Xing), wangbaojun@tyut.edu.cn (B. Wang), rfli@tyut.edu.cn (R. Li).

https://doi.org/10.1016/j.fuproc.2019.106302
Received 26 July 2019; Received in revised form 1 November 2019; Accepted 23 November 2019

H-SAPO-34. In addition, the difference in acid strength and acid distribution could be attributed to the topological differences in both the H-SAPO-34 and H-ZSM-5 [24]. Therefore, modification with heteroatoms has been employed to increase the catalytic activity and product selectivity towards light olefins, especially towards ethylene, of these zeolites by optimizing the acidity, altering the pore structure and catalytic action [22,25].

The incorporation of transition metal ions into framework sites of the zeolite is of particular interest for designing novel catalysts exhibiting special catalytic activities [19]. Metal heteroatoms have been used to increase the catalytic activity and product selectivity towards light olefins over aluminophosphates or silicoaluminophosphates [25–35] and H-ZSM-5 [22,36–39] for MTO catalytic conversion. Xu et al. [25] studied the effect of different metals on the catalytic performance of MeAPO-34 for MTO and the results showed that the incorporation of metals had a significant effect on the structure and acidity of zeolite, and improved the lifetime of catalysts or/and their selectivity towards light olefins. Tian et al. [40] synthesized modified Ce-SAPO-34 catalysts, which represented the optimum modification effect and improved the ethylene selectivity by 10 mol%. Hadi et al. [41] reported that Ce is a promising promoter for Mn/H-ZMS-5 in methanol conversion to propylene. The selectivity towards propylene was dramatically enhanced, whereas the propylene/ethylene ratio increased due to Ce doping. Zhao et al. [42] and Song et al. [43] reported that H-ZSM-5 modified by Ce, Ti and Zr possessed the adjusted pore structure and acidic properties, exhibited a high catalytic activity and enhanced the selectivity of light olefins, such as ethylene and propylene (about 64%). The catalytic properties of these materials, combined with the acidity of zeolite, give rise to bifunctional catalysts [44]. The performances of MTO conversion over these catalysts were different according to the properties of metals. Therefore, it is suggested that beside selecting a molecular sieve with a different topology, the most straightforward way to change the acid strength of acid sites is to use isomorphous substitution of elements having different properties in the framework of molecular sieves.

The ZrO_2 has showed high relevant activity and olefin selectivity in non-oxidative dehydrogenation of C_3 and C_4 alkanes [45,46]. The next step is to study the catalytic performance of MTO conversion over Zr-modified molecular sieves. To the best of our knowledge, only a handful of studies have been reported on the modification of H-SAPO-34 [31] and H-ZSM-5 [42,43] using zirconium. Furthermore, studies related to the isomorphous substitution of Zr atom in H-SAPO-34 and H-ZSM-5 used for the catalytic performance of MTO process are scarce. In the present work, the effect of the incorporation of Zr into AlPO-34 and H-ZSM-5, especially, on its pore structure, acidity and catalytic performance in the MTO reaction has been investigated. The acid strength of acid sites is determined using NH_3 adsorption energy. The present work deals with MTO conversion over Zr-modified AlPO-34 and H-ZSM-5 and compares the catalytic performances of these materials with each other and with that of unmodified H-SAPO-34 and H-ZSM-5. In other words, the influence of the framework structure of H-SAPO-34 has been investigated compared to H-ZSM-5 on the activity and selectivity of MTO conversion based on the alkene-based cycle. Furthermore, in order to demonstrate the acid strength of molecular sieve frameworks on the activity and selectivity of MTO reaction, Zr-doped AlPO-34 and H-ZSM-5 models were used to illustrate the role of acid strength. The aim of this investigation is to improve the understanding of the relationship between the catalytic performance (activity and selectivity to ethylene) and the pore structure/acid strength of H-SAPO-34, H-ZSM-5, H-ZrAPO-34 and H-Zr-ZSM-5 catalysts used for the MTO conversion. The results are expected to help in optimizing the reaction of methanol to olefins.

2. Methodology

2.1. Computational model

The H-SAPO-34 and AlPO-34 frameworks are represented by periodic 36 T hexagonal cells. The unit cell of H-SAPO-34 catalyst is derived from the CHA structure (all Si atoms are equivalent in symmetry), in which all the Si atoms are first substituted by P and Al atoms alternately, and one P atom is replaced by a Si atom to generate one Brönsted acid site at the O2 position per cage. It is worth mentioning that H-SAPO-34 is a small-pore material, in which spacious cavities (10.0 Å × 6.7 Å) are connected through small (3.8 Å × 3.8 Å) 8-ring windows [23]. For H-ZrAPO-34 catalyst, isomorphous substitution of P atom with Zr atom into AlPO-34 confers a negative charge on the framework, which uses the proton to charge-balancing at the O2 position that acts as a Brönsted acid site. The optimized lattice constants for H-SAPO-34 are: a = b = 13.85 Å and c = 15.08 Å, which are in good agreement with the results reported by Wang et al. (a = b = 13.80 Å and c = 15.04 Å) [47] and are similar to the experimental results (a = b = 13.73 Å, c = 15.05 Å) [48]. Additionally, for AlPO-34, the optimized lattice constants are: a = b = 13.53 Å, and c = 14.75 Å, which are also in good agreement with the results reported by Wang et al. (a = b = 13.90 Å and c = 15.11 Å) [49]. H-ZSM-5 has the MFI topology, exhibiting a 3D network consisting of sinusoidal (5.1 Å × 5.5 Å) and straight (5.3 Å × 5.6 Å) channels defined by 10-rings that result in medium-sized pores [23]. There exist 12 crystallographically nonequivalent T atom positions in a unit cell ($Si_{96}O_{192}$) [50]. The optimized lattice parameters (a = 20.37 Å, b = 20.08 Å and c = 13.51 Å) in a previous work [51] are in very good agreement with those reported in the IZA database (a = 20.09 Å, b = 19.74 Å and c = 13.14 Å) and some other studies [23]. Then, the periodic boundary conditions are employed. The periodic approach is the most reasonable model which can consider the limitation of TO_4 unit caused by long-range electrostatic interaction and isomorphic substitution of zeolite framework and provide a more realistic description to study the properties of a crystal [52,53]. In an earlier analysis [51], it was found that T7 is the most favorable site for the substitution of Al atom according to the stability analysis, as a result of which, a charge-balancing proton is produced at O1 positions. Therefore, in the rest of the calculation process, single substituted Al is used at T7 position. This way, the most stable structure of Zr doped H-ZSM-5 is confirmed by considering the T atom, which is adjacent to T7, and is substituted by the Zr atom. The optimized configurations of H-SAPO-34, H-ZSM-5, H-ZrAPO-34 and H-Zr-ZSM-5 are shown in Fig. 1. Full structural optimization and the cell parameters are all relaxed in order to investigate the structural deformation of Zr-doped molecular sieves. Additionally, the optimized method uses the conjugate gradient algorithm.

2.2. Methods

All the density functional theory (DFT) calculations are performed using the Perdew-Burke-Ernzerhof (PBE) exchange-correlation functional [54] as implemented in the Vienna Ab Initio Simulation Package (VASP) [55–58]. The projected augmented wave (PAW) method is used to describe the electron-ion interactions [59,60]. The cutoff energy of the planar waves is equal to 400 eV. Only a Γ point is used for the sampling of Brillouin zone [61]. Van der Waals interactions are described using the dispersion-corrected DFT-D2 method [62]. The climbing image nudged elastic band (CI-NEB) method is used to determine the minimum energy path and to locate all the transition-state structures [63]. The nature of transition states is confirmed by determining the vibrational frequencies using the finite difference method. Small displacements of 0.02 Å are used to determine the numerical Hessian matrix. All the calculated energies are corrected for zero-point energies (ZPE) due to the restricted optimizations [64,65]. Convergence is assumed have been achieved when the forces on each

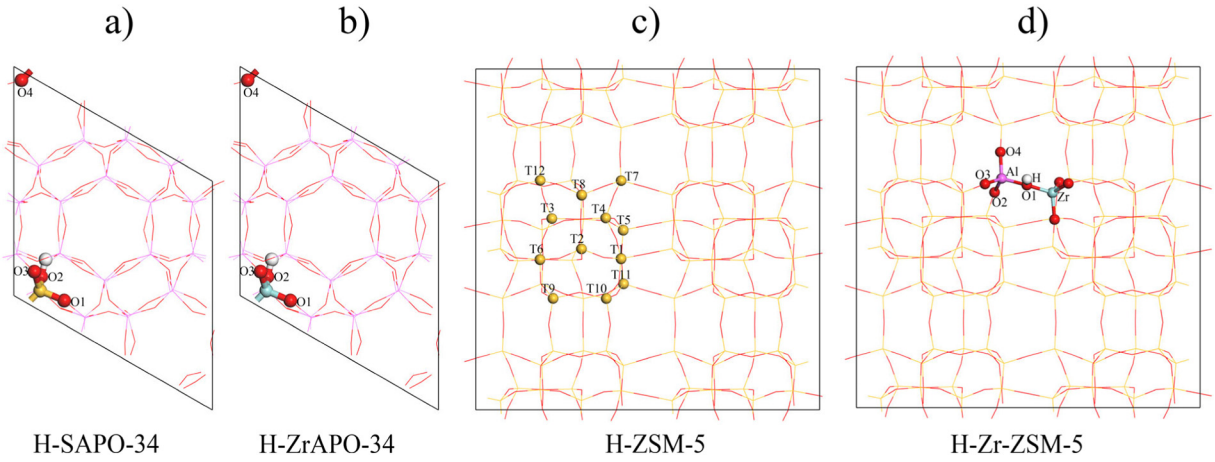

Fig. 1. The optimized configurations of a) H-SAPO-34, b) H-ZrAPO-34, c) H-ZSM-5 and d) H-Zr-ZSM-5.

atom are less than 0.05 eV $Å^{-1}$.

3. Results

3.1. Influence of heteroatom doping on the structure of AlPO-34 and H-ZSM-5

In order to simulate different acid sites corresponding to different acid strengths, P atom in the AlPO-34 framework with the Al/P ratio of 1:1 is substituted by Si and Zr atoms. Furthermore, Si atom which is around Al atom site in H-ZSM-5 framework is substituted by the Zr atom. The calculated geometrical parameters show that the bond length of Zr—O (about 2.0 Å) is longer than that of Si—O and P—O bond lengths (about 1.64 Å and 1.54 Å, respectively). Therefore, the largest deformation occurs around the substituted T atom. The substitution of P atom in AlPO-34 and that of Si atom in H-ZSM-5 structures lead to the expansion of corresponding tetrahedron, which is also accompanied by a deformation of its shape due to the reason that the compensating proton may still be located on any of the four neighboring framework oxygens. The local coordination environment around T atom in the framework can be significantly different for different location sites of heteroatom and the species of substituted heteroatom in the framework. By calculating two parameters of Θ and Ω, the degree of distortion of [TO_4] tetrahedron after the substitution of heteroatom can be understood [66–68]. The parameter Θ is the root mean square deviation, and is defined using Eq. (1) [66,67]:

$$\Theta = \sqrt{\frac{1}{6}\sum_{i=1}^{6}(\alpha_i - \overline{\alpha})^2} \quad (1)$$

where α_i represents the i^{th} θ(O − T − O) angle and $\overline{\alpha}$ is the average of the six θ(O − T − O) angles. The Θ is not a direct measure of the distortion caused by the incorporation of heteroatoms into the framework positions of zeolites [68]. The changes in local [TO_4] geometries caused by the heteroatom substitution can be quantified using the parameter Ω [68] as given by Eqs. (2)–(4).

$$\Omega_{Si} = (\Theta_{Si} - \Theta_P)/\Theta_P \quad (2)$$

$$\Omega_{Zr} = (\Theta_{Zr} - \Theta_P)/\Theta_P \quad (3)$$

$$\Omega_{Zr-ZSM5} = (\Theta_{Zr} - \Theta_{Si})/\Theta_{Si} \quad (4)$$

where Θ_{Si} and Θ_{Zr} are the average root mean square deviations from regular tetrahedron for Si and Zr atoms' substitutions, respectively. It should be noticed that Θ_P of [PO_4] tetrahedron in AlPO-34 configuration is calculated. The root mean square deviation parameter (Θ) and the parameter Ω for each substitution of AlPO-34 and H-ZSM-5 framework are presented in Table 1.

Table 1
The calculated Θ and Ω for [TO_4] (T = Si, Zr) tetrahedron of AlPO-34 and H-ZSM-5 frameworks.

Structures	Θ/°	Ω
H-SAPO-34	7.11	4.08
H-ZrAPO-34	16.27	10.62
H-Zr-ZSM-5	4.34	0.02

It can be seen from the results presented in Table 1 that the values of the parameter Θ for Si and Zr atoms' substitutions are 7.11 and 16.27 in AlPO-34 structure, respectively. The corresponding values for the parameter Ω are 4.08 and 10.62, respectively. The results indicate that the deformation of [TO_4] tetrahedron is caused by the heteroatom substitution, which results in the cavity changes of H-SAPO-34 and H-ZrAPO-34, especially the substitution of Zr atom. The calculated cavity volumes of H-SAPO-34 and H-ZrAPO-34 are 2023.25 $Å^3$ and 2238.95 $Å^3$, respectively. In other words, the cavity volumes of H-ZrAPO-34 are larger than that of H-SAPO-34. It can be concluded that there is a large space of cavities in H-ZrAPO-34. Additionally, the parameters Θ and Ω for the substation of Zr atom are 4.34 and 0.02 in H-ZSM-5, respectively. The calculated results show that the substitution of Zr atom has negligible effect on the structural deformation of [TO_4] in the H-ZSM-5 framework. This may be due to the large cavity of H-ZSM-5. The calculated cavity volumes for H-ZSM-5 and H-ZSM-5-Zr are 5480.67 $Å^3$ and 5494.76 $Å^3$, respectively. The incorporation of Zr atom into the H-ZSM-5 framework slightly increases the cavity space.

3.2. Influence of heteroatom doping on the acid strength of AlPO-34 and H-ZSM-5

In this work, the acid strengths of AlPO-34 and H-ZSM-5 are modulated by isomorphic substitution of one P atom by Si and Zr atoms in the AlPO-34 and one Si atom by Zr atom in the H-ZSM-5. The acidities of molecular sieves are investigated by determining the adsorption energy of NH_3. The adsorption energy of NH_3 (ΔE_{ads}) is given by Eq. (5) [69]:

$$E_{ads} = E_{HZ+NH_3} - E_{NH_3} - E_{HZ} \quad (5)$$

where E_{HZ+NH_3} is the calculated energy of the given geometry containing the catalyst and the adsorbed molecule, E_{HZ} is the energy of the framework itself and E_{NH_3} is that of free NH_3. It is obvious that the acid site with stronger acidity would have larger adsorption energy, which means that larger the adsorption energy, stronger is the acidity of the Brönsted acid site. The configurations of NH_3 adsorption on catalysts are shown in Fig. 2 and the corresponding calculated results are listed in Table 2.

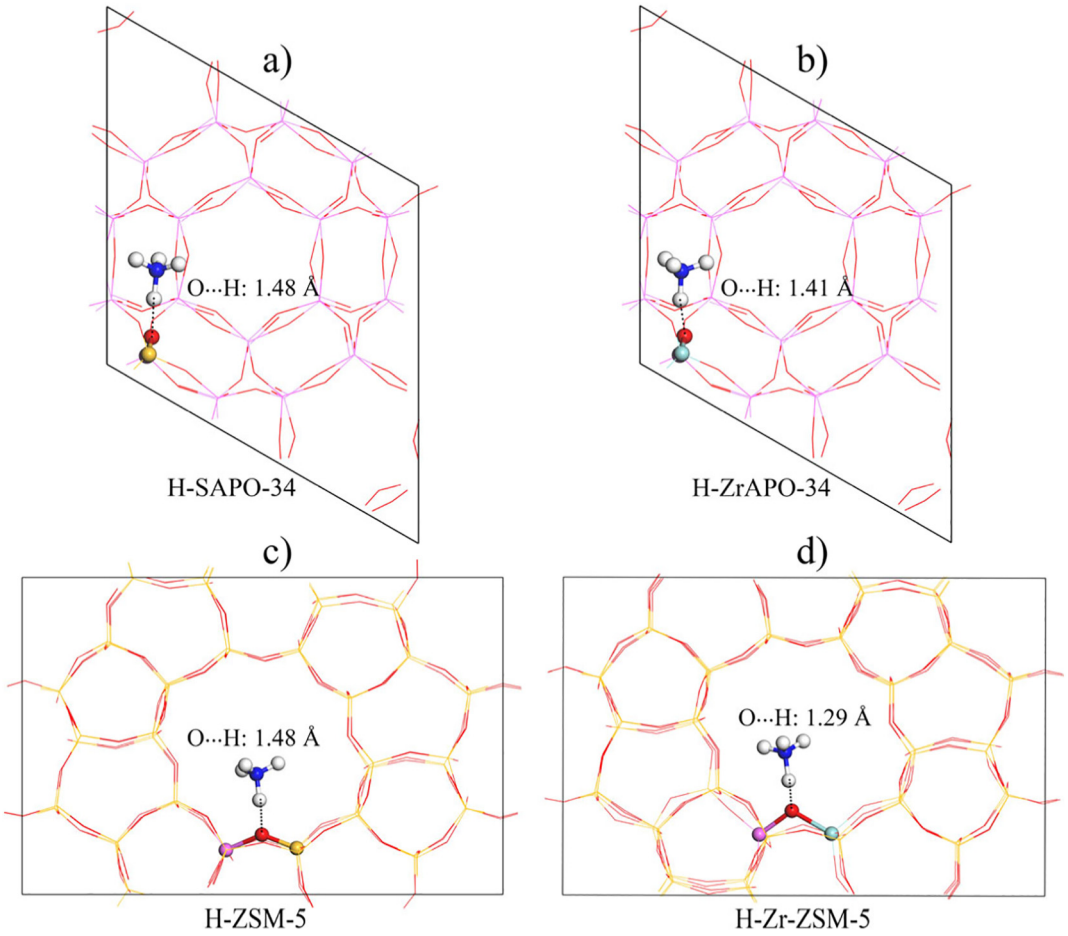

Fig. 2. The adsorption configurations of NH_3 molecule over H-SAPO-34, H-ZrAPO-34, H-ZSM-5 and H-Zr-ZSM-5.

Table 2
The adsorption energies of NH_3 (E_{ads}) over H-SAPO-34, H-ZrAPO-34, H-ZSM-5 and H-Zr-ZSM-5.

Structures	Acid site	E_{ads}/eV
H-SAPO-34	Si-O(H)-Al	−1.10
H-ZSM-5	Si-O(H)-Al	−1.10
H-ZrAPO-34	Zr-O(H)-Al	−1.00
H-Zr-ZSM-5	Si-O(H)-Al	−0.70

As shown by the results given in Table 2, the results of NH_3 adsorption energy illustrate that H-SAPO-34 and H-ZSM-5 have almost the same strengths of acid sites. However, Zr-incorporated AlPO-34 and H-ZSM-5 exhibit smaller adsorption energies of NH_3. The calculated results indicate that Zr-containing AlPO-34 and H-ZSM-5 structures exhibit weaker strengths of acid sites. Furthermore, the strength of acid site for the H-ZrAPO-34 catalyst is weaker than that of H-SAPO-34 catalyst. However, the acid strength increased with the increase in incorporated content of Zr in H-SAPO-34. The experimental results reported by Aghaei et al. [70] indicated that the acid strength increased with the increase of Zr content.

3.3. Catalytic performance of H-SAPO-34, H-ZrAPO-34 and H-ZSM-5 with and without Zr

3.3.1. Alkene-based cycles route

The full catalytic cycle for methanol to light olefin (ethylene and propylene) conversion starting from 2, 3-dimethyl-2-butene (iso-C6) is summarized in Scheme 1. As shown in Scheme 1, the iso-C6-based cycle includes a series of elementary steps, such as methylation (M1, M2, M3), deprotonation (D1, D2), shift of methyl groups (C1, C2) and cracking of alkyl chain (E1, E2) to produce light olefins [13]. In the calculations, the activation energy barrier (E_a) is calculated as the energy difference between the transition state (E_{TS}) and initial state (E_{IS}) for different reaction steps according to the correlation: $E_a = E_{TS} - E_{IS}$. The reaction enthalpy (ΔH) is calculated as the energy difference between the final state (E_{FS}) and the initial state (E_{IS}) as given by the correlation: $\Delta H = E_{FS} - E_{IS}$ [39].

All the reaction steps are divided into three groups to simplify the following statement.

3.3.1.1. Step 1. The olefin methylation consists of Reaction Eqs. (M1)–(M3)

$$(CH_3)_2C = C(CH_3)_2 + CH_3OH + HZ \rightarrow (CH_3)_3C^+ = C(CH_3)_2 + H_2O + Z^- \quad \text{(M1)}$$

$$(CH_3)_3C - C(CH_3)(CH_2) + CH_3OH + HZ \rightarrow (CH_3)_3C^+ - C(CH_3)(CH_2CH_3) + H_2O + Z^- \quad \text{(M2)}$$

$$(CH_3)_3C - C(CH_3)(CHCH_3) + CH_3OH + HZ \rightarrow (CH_3)_3C^+ - C(CH_3)(CH_3CHCH_3) + H_2O + Z^- \quad \text{(M3)}$$

The activation of CH_3OH is an important reaction step for the growth of carbon chain for different hydrocarbon pool species [5,71–73]. The methylation of iso-C6 molecule with methanol (M1) is the first step of this cycle. The first C−C bond is formed when the CH_3OH molecule attacks the iso-C6 molecule, as a result of which, the C−O bond is broken and the OH group of CH_3OH molecule interacts

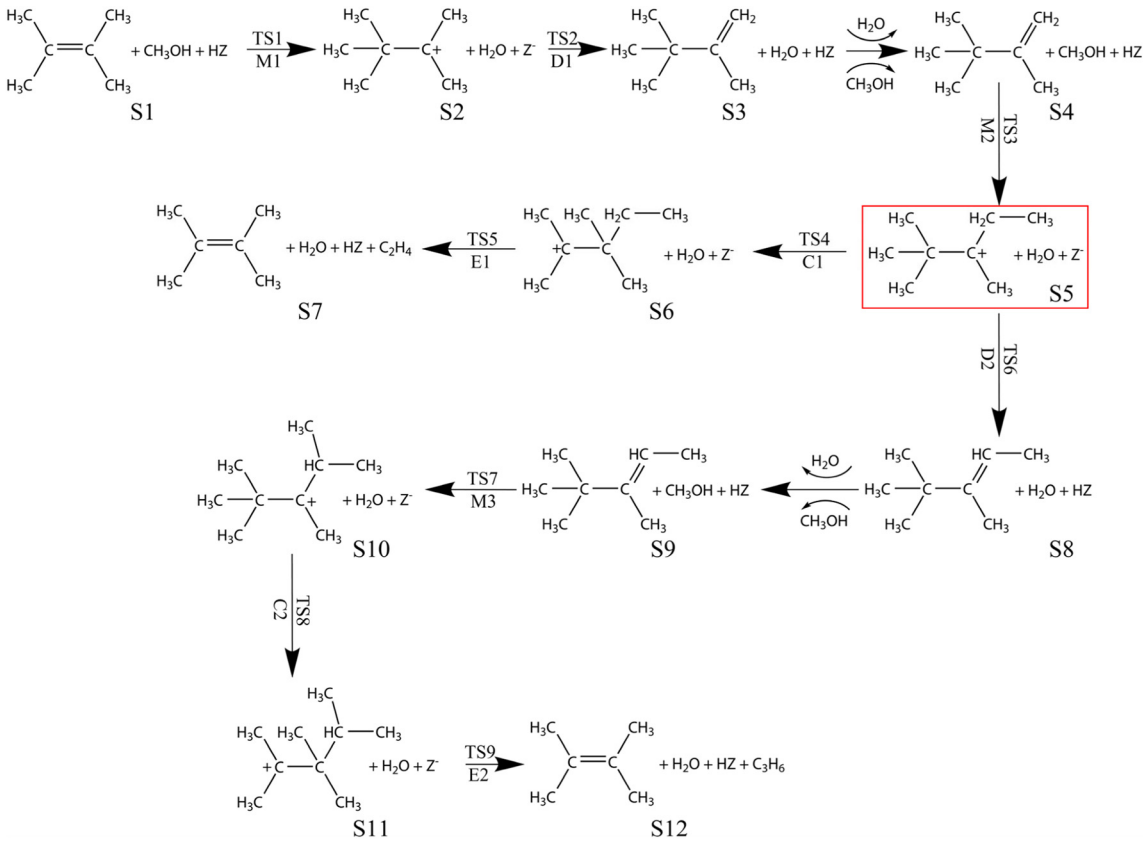

Scheme 1. The reaction pathway of alkene-based cycle for the MTO conversion.

with the proton H of acid site, thus forming an H_2O molecule, which is the result of a synergistic effect. In other words, the CH_3OH molecule attacks the iso-C6 molecule to form 2, 2, 3-trimethyl-3-butyl carbenium ion (S2) for the growth of carbon chain. In the second and third methylation steps (M2 and M3), the CH_3OH molecule attacks the double bond of 2, 2, 3-trimethyl-3-butenyl (S4) and 2, 2, 3-trimethyl-3-pentenyl (S9) species, which are generated due to the deprotonation of species S2 and 2, 2, 3-trimethyl-4-pentyl carbenium ion (S5), respectively. In M2 and M3, S4 and S9 species interact with CH_3OH molecule, respectively.

3.3.1.2. Step 2. Deprotonation of carbenium ions and the shift of methyl groups, which consist of Reaction Eqs. (D1), (D2), (C1) and (C2).

$$(CH_3)_3C^+ - C(CH_3)_2 + H_2O + Z^- \rightarrow (CH_3)_3C - C(CH_3)(CH_2) + H_2O + HZ \quad \text{(D1)}$$

$$(CH_3)_3C^+ - C(CH_3)(CH_2CH_3) + H_2O + Z^- \rightarrow (CH_3)_3C - C(CH_3)(CHCH_3) + H_2O + HZ \quad \text{(D2)}$$

$$(CH_3)_3C^+ = C(CH_3)(C_2H_5) + H_2O + Z^- \xrightarrow{CH_3\ \text{transfer}} (CH_3)_2C = C^+(CH_3)_2(C_2H_5) + H_2O + Z^- \quad \text{(C1)}$$

$$(CH_3)_3C^+ = C(CH_3)(C_3H_7) + H_2O + Z^- \xrightarrow{CH_3\ \text{transfer}} (CH_3)_2C = C^+(CH_3)_2(C_3H_7) + H_2O + Z^- \quad \text{(C2)}$$

Both the D1 and D2 are the deprotonation steps. The reaction species S2, S5 and H_2O molecule, which are generated from the methylation of M1 and M2, are considered to be adsorbed in the molecular sieve and serve as the co-reactants for each deprotonation step (D1 and D2). The H_2O molecule plays the role of "bridge" that can facilitate the proton transfer. In other words, it interacts with the proton of terminal CH_3 or CH_2CH_3 group in S2 or S5 to form S3 or S8 containing a double bond. Meanwhile, one proton (H) of H_2O molecule shifts to the acid site and regenerates the acid site of molecular sieve framework. Both the C1 and C2 are the intramolecular shift steps of methyl group, in which the CH_3 group of the first/third methylation species shifts to the next neighboring C atom. The species of 2, 2, 3-trimethyl-4-pentyl carbenium ion (S6) and 2, 3-dimethyl-2-isopropyl carbenium ion (S11) can initiate the following olefin elimination steps (ethylene elimination (E1) and propylene elimination (E2)).

3.3.1.3. Step 3. Elimination of olefins, which consists of Reaction Eqs. (E1) and (E2).

$$(CH_3)_2C = C^+(CH_3)_2(C_2H_5) + H_2O + Z^- \rightarrow C_6H_{12} + C_2H_4 + H_2O + HZ \quad \text{(E1)}$$

$$(CH_3)_2C = C^+(CH_3)_2(C_3H_7) + H_2O + Z^- \rightarrow C_6H_{12} + C_3H_6 + H_2O + HZ \quad \text{(E2)}$$

Both the E1 and E2 are the elimination steps of ethylene and propylene. Two different reaction pathways for this reaction steps are considered. Considering the elimination of ethylene, the first reaction pathway can be described as follows.

$$(CH_3)_2C = C^+(CH_3)_2(C_2H_5) + H_2O + Z^- \rightarrow C_6H_{12} + {C_2H_5}^+ + H_2O + Z^- \rightarrow C_6H_{12} + C_2H_4 + H_2O + HZ$$

This reaction pathway starts with the breaking of C—C bond in S6 species. Then, the proton of ${C_2H_5}^+$ species shifts to the original acid site to regenerate the Brönsted acid site. However, the configuration of iso-C6 and ${C_2H_5}^+$ species cannot co-exist during the calculations. Even the ${C_2H_5}^+$ species is assigned far away from the iso-C6 molecule. It is still re-bonded with the iso-C6 molecule that forms the S6 species after optimization. Therefore, this reaction pathway is excluded.

Another reaction pathway starts with the regeneration of Brönsted

acid site, which can be described as follows.

$$(CH_3)_2C = C^+(CH_3)_2(C_2H_5) + H_2O + Z^- \rightarrow (CH_3)_2C = C(CH_3)_2(C_2H_4) + H_2O + HZ \rightarrow C_6H_{12} + C_2H_4 + H_2O + HZ$$

In other words, the proton of S6 species shifts to H_2O molecule, whereas one H atom of H_2O molecule shifts to the molecular sieve framework to regenerate the acid site. Then, the C_2H_4 molecule is generated from the breaking of C—C bond between the carbon of iso-C6 and the carbon of alkyl chain. However, the results show that the C_2H_4 molecule is automatically eliminated if, at the same time, the proton is separated from the S6 species. The elimination of C_2H_4 molecule, proton transfer and the regeneration of Brönsted acid site occurred simultaneously. For the elimination step of olefin, the water molecule participates in the synergy and facilitates the proton transfer between the intermediates and molecular sieve framework. The same trend, as shown in Scheme 1, is reported by Wang et al. et al. [13]. From the intermediate species S5, where the ethylene and propylene producing cycles bifurcate, is indicated with a red box in Scheme 1. The E1 occurs through a concerted mechanism, in which the C—C bond breaks and the terminal methyl group of the ethyl group is deprotonated. During this concerted step, ethylene is split and the initial iso-C6 molecule is restored, thus closing the catalytic cycle. The propylene formation route is mechanistically similar to the ethylene formation route. However, the ethyl group of S5 species undergoes sequential deprotonation and methylation.

3.3.2. Full catalytic cycle on the H-SAPO-34 and H-ZSM-5

A catalytic reaction is considered across different frameworks and acid strengths. The corresponding configurations and the main geometrical parameters of the initial state (IS), transition state (TS) and final state (FS) or intermediate species (S1∼S12) over H-SAPO-34 and H-ZSM-5 are shown in the Supporting Information (SI).

Furthermore, the corresponding activation energy barriers and the reaction enthalpies for each step are listed in Table 3. Based on the isoC6-based cycle over H-SAPO-34 and H-ZSM-5, the energy diagrams of MTO conversion are shown in Fig. 3.

3.3.2.1. Step 1: methylation reaction. Methanol adsorption at the acid site is the first step of MTO conversion. The adsorption energy of methanol in H-SAPO-34 is calculated to be −0.95 eV. This result is in-line with the result (about −0.90 eV) obtained by David et al. [74] and Wang et al. [47]. The transition state structures of the methylation steps show that the new C—C bond formation, accompanied by the methanol dehydration, forms the higher carbenium ion. Considering the M1 over H-SAPO-34, the distance of C_2-O_1 is 2.10 Å, whereas that of C_1-C_2 is 2.48 Å in the TS, as shown in Fig. S1 in the Supporting Information.

Table 3
The activation energy barriers (E_a, eV) and the reaction enthalpies (ΔH, eV) of each step for MTO conversion over H-SAPO-34, H-ZrAPO-34, H-ZSM-5 and H-Zr-ZSM-5.

Reaction steps	H-SAPO-34		H-ZrAPO-34		H-ZSM-5		H-Zr-ZSM-5	
	E_a	ΔH	E_a	ΔH	E_a	ΔH	E_a	ΔH
M1	0.94	−0.12	0.81	−0.22	0.79	−0.06	0.69	0.11
D1	0.13	−0.39	0.19	−0.60	0.04	−0.34	0.10	−0.50
M2	1.08	0.37	1.10	0.30	1.12	−0.21	1.14	−0.77
C1	0.13	−0.38	0.15	−0.36	0.05	−0.45	0.61	0.24
E1	1.33	−0.04	0.64	0.17	1.14	0.56	0.99	0.34
D2	1.00	−0.25	0.31	−0.50	0.03	−0.75	0.05	−0.38
M3	0.97	0.33	1.05	0.28	0.96	−0.12	1.13	−0.31
C2	0.32	0.11	0.36	0.32	0.13	−0.30	0.21	−0.15
E2	0.10	−0.40	0.09	−0.90	0.82	0.10	0.73	−0.11

Similar to the H-SAPO-34, the structure of TS over H-ZSM-5 is also identified and the C_2-O_1 bond (1.46 Å) breaks along with the migration of CH_3 group from O_1 to C_1 ($r_{C1\text{-}C2}$ = 2.34 Å). Similarly, for the transition state structures of M2 and M3, the bond distances of C_1-C_2 are about 2.17–2.31 Å in H-SAPO-34 and about 2.51–2.54 Å in H-ZSM-5, which are nearly identical in all cases. Consequently, the activation energy barriers of M1, M2, M3 are determined to be 0.94, 1.08 and 0.97 eV over H-SAPO-34, respectively. This is in-line with the theoretical results reported by Wang et al. (about 0.85 eV) [13]. In addition, the same tendency is obtained over H-ZSM-5, which shows that the activation energy barriers of M1, M2 and M3 are 0.79, 1.13 and 0.96 eV, respectively. Therefore, it is confirmed that the structural features of transition state over H-SAPO-34 are similar to those over H-ZSM-5 except that the activation energy barrier of the methylation reaction and the breaking/forming bond distances vary slightly.

3.3.2.2. Step 2: deprotonation of carbenium ions and the shift of methyl groups. After the methylation step, carbenium ions are formed, which can be easily converted by deprotonation and methyl group shifts. As shown in Fig. S1 in the Supporting Information, the bond distances of C_1-H_1 are 1.32 Å and 1.70 Å in the TS structures of D1 and D2 over H-SAPO-34, respectively. Corresponding to the TS structures of D1 and D2 over H-ZSM-5, which are shown in Fig. S3 in the Supporting Information, the bond distances of C_1-H_1 are 1.27 Å and 1.59 Å, respectively. The activation energy barriers of D1 and D2 are 0.13 eV and 1.00 eV, respectively, which are higher than those over H-ZSM-5 (0.04 eV and 0.03 eV for D1 and D2, respectively). The bond distances of C_1-C_2 are 1.82 Å and 1.88 Å, whereas those of C_1-C_3 are 1.85 Å and 1.81 Å in the TS structures of C1 and C2 over H-SAPO-34, respectively. Corresponding to the TS structures of C1 and C2 over H-ZSM-5, the bond distances of C_1-C_2 are 1.84 Å and 1.93 Å, whereas those of C_1-C_3 are 1.84 Å and 1.76 Å, respectively. The activation energy barriers of C1 and C2 are 0.13 eV and 0.32 eV, respectively, which are higher than those over H-ZSM-5 (0.05 and 0.13 eV for C1 and C2, respectively). The deprotonation of carbenium ions and the shift of methyl groups need lower activation energy barriers over H-ZSM-5, which is accordance with the results obtained by David et al. [74]. It is suggested that the interactions between zeolite framework and adsorbed species play a key role in determining the catalytic reactivity. It should be mentioned that the deprotonation of carbenium ions and the shift of methyl groups, as achieved in this step, are not the most difficult kinetic steps and therefore, should not be the rate determining step for the formation of olefins.

3.3.2.3. Step 3: elimination of olefins. As mentioned earlier, the framework structure of molecular sieve can affect the deprotonation of carbenium ions and shifting of methyl group in the alkene-based cycle. The influence of framework structure of molecular sieve on the elimination of light olefins is also investigated in this work. The structure of transition state indicated that the C_1-C_2 bond breaks along with the formation of light olefins. In the case of E1 over H-SAPO-34, the bond of C_1-C_2 increases from 1.57 Å of absorbed state to 2.79 Å of TS. Furthermore, the activation energy barrier of the cracking step is 1.33 eV. In contrast, the bond of C_1-C_2 increases from 1.56 Å to 2.88 Å for E2 in TS over H-SAPO-34. This is in good agreement with the previously reported theoretical results [13]. However, the elimination of propylene requires the activation energy barrier of more than 0.10 eV. It is evident that the formation of ethylene needs higher activation energy barriers than propylene. The bond distances of C_1-C_2 are 2.56 Å and 2.88 Å in the TS structures of E1 and E2 over H-ZSM-5, respectively. The activation energy barriers of the E1 and E2 over H-ZSM-5 are 1.14 eV and 0.81 eV, respectively. The results show that, considering the elimination of olefins over H-SAPO-34 and H-ZSM-5, E2 is easier to occur over H-SAPO-34 than over H-ZSM-5, whereas E1 may be easier to occur over H-ZSM-5 than over H-SAPO-34. It is suggested that the framework structure of molecular sieve offers additional

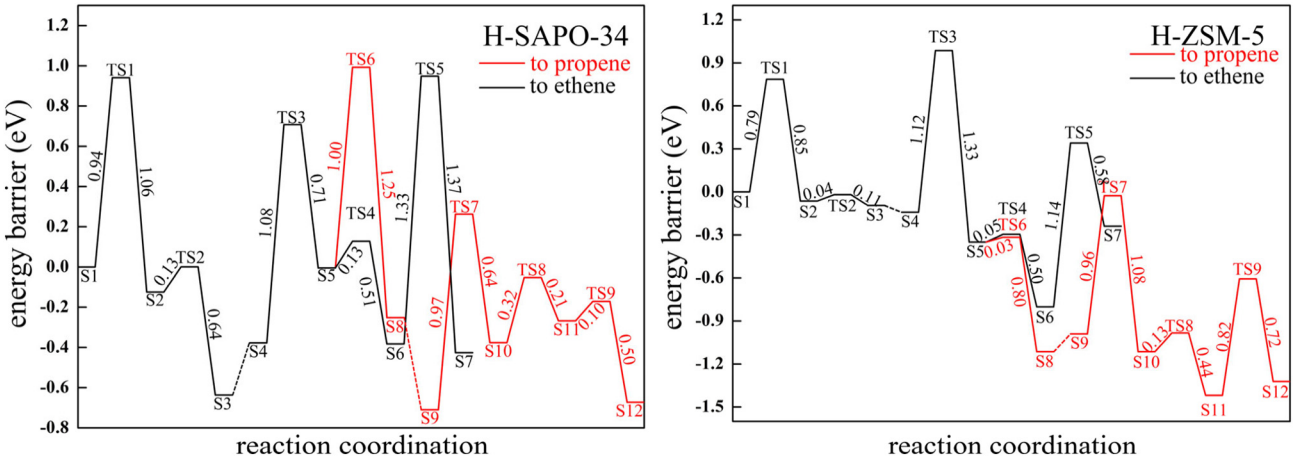

Fig. 3. The energy diagrams of the MTO conversion over H-SAPO-34 and H-ZSM-5. The cycle consists of alkyl chain propagation and ethylene elimination (in black), and propylene elimination (in red). (For interpretation of the references to colour in this figure legend, the reader is referred to the web version of this article.)

stabilization to transition states, and the relativities of the deprotonation of carbenium ions, shifts in methyl group and the cracking reactions are more sensitive to molecular sieve framework. According to the calculated results of NH_3 adsorption energy, H-SAPO-34 and H-ZSM-5 have the same acid strengths. Therefore, it is probably due to the difference in framework structures of H-SAPO-34 and H-ZSM-5, which leads to the difference in activities of MTO conversion.

3.3.3. Full catalytic cycle over H-ZrAPO-34 and H-Zr-ZSM-5

Besides the framework structure, the acid strength of molecular sieves also affects the reactivity. Therefore, the influence of acid strength on the activity and selectivity of MTO conversion is explored in this work. The models with different acid strengths of H-ZrAPO-34 and H-Zr-ZSM-5 are used. The calculated energy profiles of isoC6-based cycle over H-ZrAPO-34 and H-Zr-ZSM-5 are shown in Fig. 4. Additionally, the activation energy barriers and the reaction enthalpies for each step are listed in Table 3.

3.3.3.1. Step 1: methylation reaction. Similar to the elucidation in H-SAPO-34 and H-ZSM-5, over H-ZrAPO-34 and H-Zr-ZSM-5, the geometries of the transition state for methylation steps are much similar to those described over H-SAPO-34 and H-ZSM-5, and involve the increase of C_2-O_1 bond distance (2.01 Å–2.36 Å) and C_1-C_2 bond distance (2.01 Å–2.54 Å) in the TS structures, as shown in Figs. S2 and S4 of the Supporting Information. Furthermore, the activation energy barriers of M1, M2 and M3 over H-ZrAPO-34 are 0.81 eV, 1.10 eV and 1.05 eV, respectively, which are slightly lower than those catalyzed over H-SAPO-34 with strong acid strengths. As summarized in Table 3, the activation energy barriers of M1, M2 and M3 over H-Zr-ZSM-5 with weak acid strength are 0.69 eV, 1.14 eV and 1.13 eV, respectively, which are close to those over H-ZSM-5 with strong acid strength.

3.3.3.2. Step 2: deprotonation of carbenium ions and the shift of methyl group. The D1 and D2 over H-ZrAPO-34 occur facilely, as they only need to overcome the activation energy barriers of 0.19 eV and 0.31 eV, respectively. The activation energy barriers of C1 and C2 are 0.15 eV and 0.36 eV, respectively. Corresponding to the TS structures of D1, D2, C1 and C2 over H-ZrAPO-34, as shown in Figs. S2 in Supporting Information, the bond distances of C_1-H_1 are 1.46 Å and 1.36 Å, while those of C_1-C_2 are 1.80 Å and 1.83 Å, respectively. Similarly, the bond distances of C_1-C_3 are 1.90 Å and 1.85 Å, respectively. The results show that the shift of hydride over H-ZrAPO-34 with weak acid strength is more advantageous than that over H-SAPO-34 with relatively strong acid strength. Furthermore, the difference in strengths and the location of acid site affect the steps of the deprotonation of carbenium ions and the shift of methyl group. As listed in Table 3, the activation energy barriers of the shifting of hydride over H-Zr-ZSM-5 with weak acid strength is close to that over H-ZSM-5 with strong acid strength. As shown in Fig. S4, corresponding to the TS structures of D1, D2, C1 and C2 over H-Zr-ZSM-5, the bond distances of C_1-H_1 are 1.25 Å and 1.27 Å,

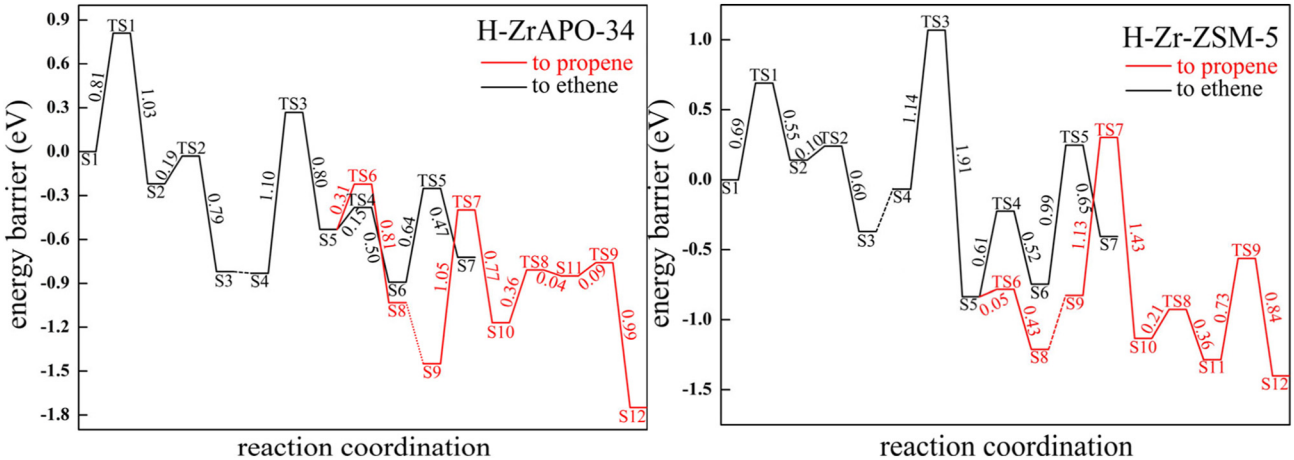

Fig. 4. The energy diagrams of the MTO conversion over H-ZrAPO-34 and H-Zr-ZSM-5. The cycle consists of alkyl chain propagation and ethylene elimination (in black), and propylene elimination (in red). (For interpretation of the references to colour in this figure legend, the reader is referred to the web version of this article.)

while those of C_1-C_2 are 1.81 Å and 1.84 Å, respectively. Furthermore, the bond distances of C_1-C_3 are 1.87 Å and 1.83 Å, respectively. These observations obviously reveal that the strength of acid site has no significant effect on the activity of methylation reaction, the deprotonation of carbenium ions and the shift of methyl group over H-SAPO-34 and H-ZSM-5.

3.3.3.3. Step 3: elimination of olefins. The influence of acid strength on the elimination of olefins is also examined in this work. For E1 over H-ZrAPO-34 needs to overcome the activation energy barrier of 0.64 eV. In other words, the activation energy barrier of E1 decreases by 0.69 eV over H-ZrAPO-34 as compared to that over H-SAPO-34 with relatively strong acid strength. Additionally, the activation energy barrier of E2 is almost the same as that catalyzed over H-SAPO-34. The calculated results indicate that the incorporation of Zr atom into AlPO-34 framework improves the whole activity of MTO conversion. In addition, the bond distances of C_1-C_2 are 2.45 Å and 3.07 Å in the TS structures of E1 and E2 over H-SAPO-34, respectively. However, as listed in Table 3, the activation energy barriers of E1 and E2 over H-Zr-ZSM-5 are 0.99 eV and 0.73 eV, which are lower than those over H-ZSM-5 with strong acid strength. Furthermore, corresponding to the TS structures of E1 and E2 over H-Zr-ZSM-5, the bond distances of C_1-C_2 are 2.57 Å and 2.77 Å, respectively.

The calculated results suggest that the stronger acidic molecular sieves are prone to produce carbenium ions as compared to weaker acidic molecular sieves. However, it is unfavorable for the elimination of olefins. Regarding the propagation of C—C chain, Brönsted acidity is closely correlated with the formation of active intermediate species (alkenes and the corresponding carbenium ions) and results in the generation of ethylene and propylene.

4. Discussion

As is known, the framework structure and the acid strength of zeolite play an important role in acid-catalyzed reactions [18,20–22,75–77]. The relationships between the framework structure/acid strength and the activity and selectivity of alkene-based MTO conversion are discussed in detail. In this work, the activities of different catalysts are determined by comparing the activation energy barriers of the rate-determining steps in the reaction coordination of the MTO conversion over H-SAPO-34, H-ZrAPO-34 and H-ZSM-5 with and without Zr atom. Furthermore, in order to verify the selectivity towards ethylene and propylene over different zeolites, the energetic span model is adopted [78]. As shown in Scheme 1, the ethylene and propylene producing cycles bifurcate and is represented by the intermediate species S5. Therefore, the energetic span model, which is employed to identify the preferred reaction mechanism and product selectivity [79], is used to analyze the product selectivity starting from S5 species. In this approach, the energetic span model is used, which enables one to evaluate the turnover frequency (TOF) of catalytic cycles based on its computed energy profile in a straightforward manner. Furthermore, TOF in affinity with the Curtin-Hammett principle [80] which is formulated to treat selectivity of reactions.

For exothermal reactions, the TOF is defined as Eq. (6) [78].

$$\mathrm{TOF} = \frac{k_B T}{h} e^{-\delta E/RT} \tag{6}$$

In addition, δE is defined as the energetic span and described using Eq. (7).

$$\delta E = \begin{cases} E_{TDTS} - E_{TDI} & \text{if TDTS appears after TDI} \quad (1) \\ E_{TDTS} - E_{TDI} + \Delta G_r & \text{if TDTS appears before TDI (2)} \end{cases} \tag{7}$$

where E_{TDTS} is the energy of TDTS, which represents the TOF-determining transition state in the energy profile of MTO conversion, and E_{TDI} is the energy of TDI, which represents the TOF-determining intermediate in the energy profile of MTO conversion, as shown in Figs. 3 and 4. In addition, the combination of TDTS and TDI should maximize the value of δE. Therefore, the TDTS and TDI may neither be the maximum and minimum energy states nor the rate-determining step in the energy profile of the MTO conversion. Herein, the energy profile of MTO conversion over H-SAPO-34 is taken as an example. As shown in Fig. 3, the TDTS and TDI are TS5 and S6 species for the ethylene formation over H-SAPO-34, respectively. Furthermore, the TDTS (TS5 species) appears after the TDI (S6 species). Therefore, the δE should be calculated using Eq. (7) 1. However, the TDTS and TDI are the TS6 and S9 species for the propylene formation over H-SAPO-34, respectively. In addition, the TDTS (TS6 species) appears before the TDI (S9 species), due to which, the δE should be calculated using Eq. (7) 2. An analogous approach is used for other catalysts. Similarly, ΔG_r is the reaction enthalpy of MTO conversion. Therefore, the δE serves as the apparent activation energy of the catalytic cycle [81] and is used to treat product's selectivity of the MTO conversion in this work. It is obviously found that, smaller the energetic span (δE), faster is the reaction [82–86], and consequently, leads to higher selectivity towards ethylene or propylene.

4.1. Influence of topological structure of molecular sieves on the activity and selectivity of MTO conversion

The MTO conversions over H-SAPO-34 and H-ZSM-5 with different topological structures are investigated. The calculated adsorption energy of NH_3 molecule indicates that the acid strength of H-SAPO-34 is almost the same as that of H-ZSM-5. Therefore, the role of topological structures on the MTO conversion is discussed in this section. Fig. 3 presents the reaction coordination of MTO conversion over H-SAPO-34 and H-ZSM-5. For a direct comparison of the activity of MTO conversions over different topological structures of H-SAPO-34 with small pore channel and H-ZSM-5 with large pore channel, the activation energy barriers of the rate-determining steps of MTO conversion are compared. As mentioned earlier, it is identified that the elimination step of ethylene (E1) is the rate-determining step in the reaction pathway of ethylene formation, while the second methylation step (M2) is the rate-determining step in the reaction pathway of propylene formation. As listed in Table 3, the activation energy barrier of E1 over H-ZSM-5 is 0.19 eV lower than that over H-SAPO-34. However, the activation energy barrier of M2 over H-ZSM-5 is only 0.04 eV higher than that over H-SAPO-34. The calculated results indicate that the activity of H-ZSM-5 for ethylene formation in MTO conversion is higher than that of H-SAPO-34, while the activities of H-SAPO-34 and H-ZSM-5 for propylene formation are almost the same. According to the calculated results, it is obvious that the higher activities of H-ZSM-5 could be attributed to large pore channel size.

Both the H-SAPO-34 and H-ZSM-5 produce products, which are mainly composed of olefins. However, there exists a significant difference in olefins' (ethylene and propylene in this work) selectivity. In other words, the selectivity ratio of propylene to ethylene can be tuned. As shown in Fig. 3, the TDTS and TDI are TS5 and S6 species for the ethylene formation over H-SAPO-34 and H-ZSM-5, respectively. Furthermore, the TDTS (TS5 species) appears after the TDI (S6 species), due to which, δE should be calculated using Eq. (7) 1. The calculated δE values are 1.33 eV and 1.14 eV for H-SAPO-34 and H-ZSM-5, respectively. The determinations of TDTS and TDI in the energy profiles of propylene formation are much more complicated than those of ethylene formation. This is due to the reason that there are more reaction steps in propylene formation cycle, and therefore, the reaction enthalpy should be considered in Eq. (7) 2. As shown in Fig. 3, the TDTS and TDI are the TS6 and S9 species for the propylene formation over H-SAPO-34, respectively. For the propylene formation over H-ZSM-5, the TDTS is the TS7 species. The TDI is the S8 species, which is not the minimum energy state in the energy profile of MTO conversion. The δE values are calculated to be 1.05 eV and 1.09 eV for the propylene formation over

H-SAPO-34 and H-ZSM-5, respectively. Based on δE analysis, it is deduced that the higher selectivity to propylene are observed over H-SAPO-34 and H-ZSM-5. However, the selectivity ratios of propylene to ethylene are different over H-SAPO-34 and H-ZSM-5. This observation over H-SAPO-34 is consistent with the results reported by Francesca Bleken et al. [87], who found that there was more propylene formation than ethylene on the carbon basis due to the reason that C_2/C_3 ratio was always lower than 0.93 over H-SAPO-34. This result is also consistent with the experimental results reported by Li et al. [17], who illustrated the relatively higher propylene selectivity over SAPO-34. Similarly, the calculated results of E1 and E2 over H-ZSM-5 are in accordance with the reported experimental data [34] for the product's selectivity over H-ZSM-5 in the MTO conversion. Fereydoon reported that the selectivity to propylene (about 48.4 mol%) is higher than that to ethylene (about 10.9 mol%) [34]. This observation is in good agreement of the report of Xu et al. [88], who found that, on the basis of unique MFI structure, a higher propylene to ethylene ratio could be achieved. It should be mentioned that the H-SAPO-34, which has nearly equal acid strength to that of H-ZSM-5, exhibits different selectivity to ethylene and propylene due to the different topological framework of H-SAPO-34 and H-ZSM-5.

4.2. Influence of Zr incorporation on the activity and selectivity of MTO conversion

The MTO conversion over H-SAPO-34, H-ZrAPO-34, H-ZSM-5 and H-Zr-ZSM-5 are conducted in order to gain further insight into the influence of Zr incorporation on the activity and selectivity of MTO conversion. The structures of IS, TS and FS for each step over H-ZrAPO-34 and H-Zr-ZSM-5 are provided in the Supporting Information. Furthermore, the corresponding activation energy barriers and the reaction enthalpy about each step are listed in Table 3. As discussed earlier, the incorporation of Zr atom into the framework of molecular sieve induces the changes in cavity structure and acid strength. Further to this, the influence of cavity structure and acid strength on the activity and selectivity in the MTO conversion are discussed in this work.

4.2.1. Activity and selectivity of MTO conversion over H-SAPO-34 and H-ZrAPO-34

The Zr-containing AlPO-34 displayed similar adsorption energy of NH_3 molecule as that of H-SAPO-34 (−1.00 eV vs. −1.10 eV), indicating that the incorporation of Zr in AlPO-34 induces little change in the acid strength. However, the modified H-ZrAPO-34 displayed noticeable differences in the pore volume, as compared to the reference H-SAPO-34, which confirms the fact that the pore volume of H-ZrAPO-34 became larger (increases by 200 $Å^3$). This observation is in good agreement with the experimental results reported by Yaripour et al. [34], who found that boron modification increased the pore volume. Pore volume is one of the significant factors influencing the catalytic activity [34]. Therefore, the influence of changes in pore volume caused by Zr incorporation on the MTO conversion is mainly discussed in this section.

The same approach is used as elucidated earlier for H-SAPO-34 and H-ZSM-5. As mentioned earlier in Section 3.3.3, it is identified that both the M2 are rate-determining steps for ethylene and propylene formations over H-ZrAPO-34, which is different from that over H-SAPO-34. As listed in Table 3, the calculated results show that the activation energy barrier of M2 over H-ZrAPO-34 is lower than that of E1 over H-SAPO-34 (1.10 eV vs. 1.33 eV). This indicates that H-ZrAPO-34 with larger cavity space has higher activity for ethylene formation. Furthermore, the activation energy difference of the elimination of propylene over H-SAPO-34 and H-ZrAPO-34 is only 0.02 eV. It is suggested that the incorporation of Zr atom into the framework of AlPO-34 structure results in a larger cavity space of H-ZrAPO-34 than that of H-SAPO-34, which is conducive to the MTO conversion that leads to higher activity.

In order to determine the selectivity of H-ZrAPO-34 to ethylene or propylene, the δE values of ethylene and propylene formation cycles are also calculated. As shown in Fig. 4, the TDTS and TDI are also the TS5 and S6 species for the ethylene formation cycle over H-ZrAPO-34. Similarly, the TDTS (TS5 species) appears after the TDI (S6 species), and the δE values are calculated to be 0.64 using Eq. (7) 1. For propylene formation cycle over H-ZrAPO-34, the TDTS is the TS7 species, which is not the highest energy state, whereas the TDI is the S9 species. The TDTS (TS7 species) appears before the TDI (S9 species), and the δE values are calculated to be 1.05 using Eq. (7) 2. Compared with the H-SAPO-34, it can be seen from the calculated results that the selectivity of H-ZrAPO-34 to ethylene is obviously enhanced. However, Zr incorporation has little effect on the selectivity to propylene. This may be due to the Zr modification that slightly decreases the acid strength, which results in an enhanced selectivity to ethylene. The calculated results suggest that the cavity-structure possesses potential to be a feasible approach to regulate the activity. Therefore, cavity-controlled activity or in other words, cavity structure determines the formation of ethylene and propylene, and in turn controls the MTO reaction activity.

4.2.2. Activity and selectivity of MTO conversion over H-ZSM-5 and H-Zr-ZSM-5

As mentioned earlier in Section 3.1, the influence of the incorporation of Zr atom into the framework of H-ZSM-5 on the pore volume is negligible. However, it significantly modifies the acid strength. It is suggested that the acid strength of H-Zr-ZSM-5 is significantly weaker than that of H-ZSM-5 (−0.70 eV vs. −1.10 eV). The Brönsted acid center plays a vital role in MTO reaction catalyzed by the zeotype catalysts. Therefore, the following discussion of the activity and selectivity of MTO conversion over H-ZSM-5 and H-Zr-ZSM-5 mainly focus on the acid strength.

Similar to the explanation in Section 3.2, the influence of acid strength on the activity of MTO conversion over H-ZSM-5 and H-Zr-ZSM-5 are also investigated. This is done based upon the analysis of activation energy barrier of the rate-determining step. It is identified that both the M2 are rate-determining steps for ethylene and propylene formations over H-Zr-ZSM-5, which is the same as that over H-ZrAPO-34. However, it is different from that over H-ZSM-5. This observation is the same as that over H-SAPO-34 and H-ZrAPO-34. Additionally, as listed in Table 3, the calculated results indicate that both the activation energy barrier of E1 over H-ZSM-5 and M2 over H-Zr-ZSM-5 are equal to 1.14 eV. Furthermore, the activation energy difference of the rate-determining steps for propylene formation cycles over H-ZSM-5 and H-Zr-ZSM-5 is only 0.02 eV. This indicates that the activities of H-ZSM-5 and H-Zr-ZSM-5 are almost the same. It can be concluded that the incorporation of Zr atom into the framework of H-ZSM-5 structure results in a weaker acid strength of H-Zr-ZSM-5 than that of H-ZSM-5, which has no obvious effect on the activity of MTO conversion.

The δE values are also calculated to compare the selectivity towards ethylene and propylene over H-Zr-ZSM-5. As shown in Fig. 4, similar to that over H-ZrAPO-34, the TDTS and TDI are the TS5 and S6 species for the ethylene formation cycle over H-Zr-ZSM-5. The TDTS (TS5 species) appears after the TDI (S6 species). The δE values are calculated to be 0.99 using Eq. (7) 1. For propylene formation cycle over H-Zr-ZSM-5, the TDTS is the TS7 species, while TDI is the S8 species, which is not the lowest energy state. The TDTS (TS7 species) appears before the TDI (S9 species). The δE values are calculated to be 1.52 using Eq. (7) 2. Compared with the H-ZSM-5, the calculated results show that the H-Zr-ZSM-5 with weaker acid strength lead to an increase in the selectivity towards ethylene in the MTO conversion. This also results in a corresponding decrease in the selectivity towards propylene. According to the calculated results, it is obvious that the more favorable selectivity to ethylene of H-Zr-ZSM-5 could be attributed to a weaker strength of acid site, which is in accordance with the results of H-ZrAPO-34. Furthermore, H-ZrAPO-34 with slight weaker acid strength represents relatively higher selectivity to ethylene. These observations are in accordance with the experimental work of Jiang et al. [18] and Yaripour

et al. [34], who found that the catalyst acidity is closely related to the product selectivity in MTO reaction and reported that the more favorable selectivity to light olefins of the catalysts could be attributed to the high amount of weak acid sites and low concentration of strong acid sites, which improved the production of light olefins.

In short, the cavity space of molecular sieve mainly affects the activity of MTO conversion. It can be concluded from the discussion of cavity change that the larger cavity space of H-ZrAPO-34 is favorable for the MTO conversion. The acid strength of molecular sieve mainly affects the selectivity of MTO conversion. Furthermore, H-Zr-ZSM-5 with weaker acid strength lead to an increase in the selectivity to ethylene as compared to that for H-ZSM-5 with strong acid strength, which leads to an increase in the selectivity to propylene. It is confirmed that decreasing the acid strength and considering pore confinement effect could decrease the activation barriers and improve the catalytic performance for MTO conversion in alkenes-based cycle.

5. Conclusions

The influence of framework's structure and acid strength on the catalytic performance of MTO conversion with the alkene-based cycle over H-SAPO-34, H-ZSM-5, H-ZrAPO-34 and H-Zr-ZSM-5 has been investigated using density functional calculations including dispersion correction. The adsorption energy of probe NH_3 molecule is used for characterizing the relative acid strength for H-SAPO-34, H-ZSM-5, H-ZrAPO-34 and H-Zr-ZSM-5. The activities of different catalysts are determined by comparing the activation energy barriers of the rate-determining steps, whereas the selectivity towards ethylene and propylene over different molecular sieves are evaluated using the calculated δE in the energy profile of MTO conversion.

For the MTO conversion on iso-C6-based cycle, the framework structure and acid strength have a significant influence on the activity and selectivity of light olefins, such as ethylene and propylene. It can be seen from the calculated results that the incorporation of Zr atom into the framework of AlPO-34 leads to an increase in the cavity space, whereas the incorporation of Zr atom into H-ZSM-5 has little effect on the cavity space. Additionally, the activity of H-ZrAPO-34 is enhanced, whereas H-Zr-ZSM-5 has little effect on the activity. The calculated results suggest that the cavity-structure can be used to regulate the activities of different catalysts. In addition, the acid strengths of H-ZrAPO-34 and H-Zr-ZSM-5 are both reduced. The acid strength of Brönsted acid site affects the product selectivity of different catalysts in the MTO conversion. Compared with H-SAPO-34 and H-ZSM-5, the considerable enhancement of selectivity towards ethylene could be attributed to the reduction of strong acid sites of H-ZrAPO-34 and H-Zr-ZSM-5. Therefore, it can be concluded that the steric constraints exerted by a larger cavity are favorable for MTO conversion, while weak acid strengths of catalysts display a higher selectivity towards ethylene.

This work will deepen the current understanding of framework's "structure/acid strengths and MTO conversion activity and selectivity over different molecular sieves, which can be used for developing more effective catalysts for MTO conversion.

Declaration of competing interest

The authors declare that they have no known competing financial interests or personal relationships that could have appeared to influence the work reported in this paper.

Acknowledgement

This work is supported by the National Natural Science Foundation of China (No. 21978192) and Shanxi Provincial Key Innovative Research Team in Science and Technology (No. 2014131006).

Appendix A. Supplementary data

Supplementary data to this article can be found online at https://doi.org/10.1016/j.fuproc.2019.106302.

References

[1] K. De Wispelaere, K. Hemelsoet, M. Waroquier, V. Van Speybroeck, Complete low-barrier side-chain route for olefin formation during methanol conversion in H-SAPO-34, J. Catal. 305 (2013) 76–80.
[2] T. Liang, J. Chen, Z. Qin, J. Li, P. Wang, S. Wang, G. Wang, M. Dong, W. Fan, J. Wang, Conversion of methanol to olefins over H-ZSM-5 Zeolite: reaction pathway is related to the framework aluminum siting, ACS Catal. 6 (2016) 7311–7325.
[3] M. Stöcker, Methanol-to-hydrocarbons: catalytic materials and their behavior, Micropor. Mesopor. Mater. 29 (1999) 3–48.
[4] W. Wang, A. Buchholz, M. Seiler, M. Hunger, Evidence for an initiation of the methanol-to-olefin process by reactive surface methoxy groups on acidic zeolite catalysts, J. Am. Chem. Soc. 125 (2003) 15260–15267.
[5] Z.H. Wei, Y.Y. Chen, S. Wang, L.I. Jun-Fen, M. Dong, Z.F. Qin, J.G. Wang, W.B. Fan, A review on the mechanism for the catalytic conversion of methanol over acid molecular sieves, J. Fuel Chem. Tech. 41 (2013) 897–910.
[6] D. Lesthaeghe, V. Van Speybroeck, G.B. Marin, M. Waroquier, Understanding the failure of direct C-C coupling in the zeolite-catalyzed methanol-to-olefin process, Angew. Chem. 118 (2006) 1746–1751.
[7] D. Lesthaeghe, V.V. Speybroeck, G.B. Marin, M. Waroquier, What role do oxonium ions and oxonium ylides play in the ZSM-5 catalysed methanol-to-olefin process?, Chem. Phys. Lett., 417 (2006) 309–315.
[8] I.M. Dahl, S. Kolboe, On the reaction mechanism for hydrocarbon formation from methanol over SAPO-34: 2. Isotopic labeling studies of the co-reaction of propene and methanol, J. Catal. 161 (1996) 304–309.
[9] I.M. Dahl, S. Kolboe, On the reaction mechanism for hydrocarbon formation from methanol over sapo-34: I. Isotopic labeling studies of the co-reaction of ethene and methanol, J. Catal. 149 (1994) 458–464.
[10] Z. Wei, Y.-Y. Chen, J. Li, W. Guo, S. Wang, M. Dong, Z. Qin, J. Wang, H. Jiao, W. Fan, Stability and reactivity of intermediates of methanol related reactions and C–C bond formation over H-ZSM-5 acidic catalyst: a computational analysis, J. Phys. Chem. C 120 (2016) 6075–6087.
[11] M. Bjørgen, S. Svelle, F. Joensen, J. Nerlov, S. Kolboe, F. Bonino, L. Palumbo, S. Bordiga, U. Olsbye, Conversion of methanol to hydrocarbons over zeolite H-ZSM-5: on the origin of the olefinic species, J. Catal. 249 (2007) 195–207.
[12] C.-M. Wang, Y.-D. Wang, H.-X. Liu, Z.-K. Xie, Z.-P. Liu, Catalytic activity and selectivity of methylbenzenes in HSAPO-34 catalyst for the methanol-to-olefins conversion from first principles, J. Catal. 271 (2010) 386–391.
[13] C.-M. Wang, Y.-D. Wang, Y.-J. Du, G. Yang, Z.-K. Xie, Similarities and differences between aromatic-based and olefin-based cycles in H-SAPO-34 and H-SSZ-13 for methanol-to-olefins conversion: insights from energetic span model, Catal. Sci. Technol. 5 (2015) 4354–4364.
[14] W. Dai, X. Wang, G. Wu, N. Guan, M. Hunger, L. Li, Methanol-to-olefin conversion on silicoaluminophosphate catalysts: effect of Brønsted acid sites and framework structures, ACS Catal. 1 (2011) 292–299.
[15] C. Wang , Y. Chu , A. Zheng, J. Xu, Q. Wang, P. Gao, G. Qi, Y. Gong, F. Deng, New insight into the hydrocarbon-pool chemistry of the methanol-to-olefins conversion over zeolite H-ZSM-5 from GC-MS, solid-state NMR spectroscopy, and DFT calculations, Chem. Eur. J., 20 (2014) 12432–12443.
[16] S. Wang, Y. Chen, Z. Wei, Z. Qin, T. Liang, M. Dong, J. Li, W. Fan, J. Wang, Evolution of aromatic species in supercages and its effect on the conversion of methanol to olefins over H-MCM-22 Zeolite: a density functional theory study, J. Phys. Chem. C 120 (2016) 27964–27979.
[17] L.I. Jinzhe, Y. Wei, G. Liu, Q.I. Yue, T. Peng, L.I. Bing, H.E. Yanli, Z. Liu, Comparative study of MTO conversion over SAPO-34, H-ZSM-5 and H-ZSM-22: correlating catalytic performance and reaction mechanism to zeolite topology, Catal. Today 171 (2011) 221–228.
[18] X. Jiang, X. Su, X. Bai, Y. Li, L. Yang, K. Zhang, Y. Zhang, Y. Liu, W. Wu, Conversion of methanol to light olefins over nanosized [Fe,Al]ZSM-5 zeolites: influence of Fe incorporated into the framework on the acidity and catalytic performance, Micropor. Mesopor. Mater. 263 (2018) 243–250.
[19] H. Zuo, Q. Xin, V. Meynen, E. Klemm, Sensitivity of the selective oxidation of methane over Fe/ZSM-5 zeolites in a micro fixed-bed reactor for the catalyst preparation method, Appl. Catal., A 566 (2018) 96–103.
[20] M. Heuchel, C. Dörr, R. Boldushevskii, S. Lang, E. Klemm, Y. Traa, The influence of porosity and active sites of zeolites Y and beta on the co-cracking of n-decane and 2-ethylphenol, Appl. Catal., A 553 (2018) 91–106.
[21] P.N. Plessow, F. Studt, Theoretical insights into the effect of the framework on the initiation mechanism of the MTO process, Catal. Lett. 148 (2018) 1246–1253.
[22] X. Li, F. Rezaei, A.A. Rownaghi, Methanol-to-olefin conversion on 3D-printed ZSM-5 monolith catalysts: Effects of metal doping, mesoporosity and acid strength, Micropor. Mesopor. Mater. 276 (2019) 1–12.
[23] C. Baerlocher, L.B. McCusker, Database of Zeolite Structures: http://www.iza-structure.org/databases/.
[24] M. Westgård Erichsen, S. Svelle, U. Olsbye, H-SAPO-5 as methanol-to-olefins (MTO) model catalyst: Towards elucidating the effects of acid strength, J. Catal. 298 (2013) 94–101.
[25] L. Xu, Z. Liu, A. Du, Y. Wei, Z. Sun, Synthesis, characterization, and MTO performance of MeAPSO-34 molecular sieves, in: X. Bao, Y. Xu (Eds.), Stud. Surf. Sci.

Catal, Elsevier, 2004, pp. 445–450.
[26] M.J. van Niekerk, J.C.Q. Fletcher, C.T. O'Connor, Effect of catalyst modification on the conversion of methanol to light olefins over SAPO-34, Appl. Catal., A 138 (1996) 135–145.
[27] M. Salmasi, S. Fatemi, A.T. Najafabadi, Improvement of light olefins selectivity and catalyst lifetime in MTO reaction; using Ni and Mg-modified SAPO-34 synthesized by combination of two templates, J. Ind. Eng. Chem. 17 (2011) 755–761.
[28] D. Zhang, Y. Wei, L. Xu, F. Chang, Z. Liu, S. Meng, B.-L. Su, Z. Liu, MgAPSO-34 molecular sieves with various Mg stoichiometries: synthesis, characterization and catalytic behavior in the direct transformation of chloromethane into light olefins, Micropor. Mesopor. Mater. 116 (2008) 684–692.
[29] F.C. Sena, B.F. de Souza, N.C. de Almeida, J.S. Cardoso, L.D. Fernandes, Influence of framework composition over SAPO-34 and MeAPSO-34 acidity, Appl. Catal., A 406 (2011) 59–62.
[30] D.R. Dubois, D.L. Obrzut, J. Liu, J. Thundimadathil, P.M. Adekkanattu, J.A. Guin, A. Punnoose, M.S. Seehra, Conversion of methanol to olefins over cobalt-, manganese- and nickel-incorporated SAPO-34 molecular sieves, Fuel Process. Technol. 83 (2003) 203–218.
[31] T. Inui, S. Phatanasri, H. Matsuda, Highly selective synthesis of ethene from methanol on a novel nickel–silicoaluminophosphate catalyst, J. Chem. Soc. Chem. Commun. (1990) 205–206.
[32] J. Chen, J.M. Thomas, MAPO-18 (M = Mg, Zn, Co): a new family of catalysts for the conversion of methanol to light olefins, J. Chem. Soc. Chem. Commun. (1994) 603–604.
[33] J.M. Thomas, Y. Xu, C.R.A. Catlow, J.W. Couves, Synthesis and characterization of a catalytically active nickel silicoaluminophosphate catalyst for the conversion of methanol to ethene, Chem. Mater. 3 (1991) 667–672.
[34] F. Yaripour, Z. Shariatinia, S. Sahebdelfar, A. Irandoukht, Effect of boron incorporation on the structure, products selectivities and lifetime of H-ZSM-5 nanocatalyst designed for application in methanol-to-olefins (MTO) reaction, Micropor. Mesopor. Mater. 203 (2015) 41–53.
[35] Y. Wei, D. Zhang, L. Xu, F. Chang, Y. He, S. Meng, B.-l. Su, Z. Liu, Synthesis, characterization and catalytic performance of metal-incorporated SAPO-34 for chloromethane transformation to light olefins, Catal. Today 131 (2008) 262–269.
[36] G. Coudurier, A. Auroux, J.C. Vedrine, R.D. Farlee, L. Abrams, R.D. Shannon, Properties of boron-substituted ZSM-5 and ZSM-11 zeolites, J. Catal. 108 (1987) 1–14.
[37] B. Kaur, M. Tumma, R. Srivastava, Transition-metal-exchanged nanocrystalline ZSM-5 and metal-oxide-incorporated SBA-15 catalyzed reduction of nitroaromatics, Ind. Eng. Chem. Res. 52 (2013) 11479–11487.
[38] J.C. Lin, K.J. Chao, W. Yu, The location of cations in Cs-exchanged ZSM-5 zeolite, Zeolites 11 (1991) 376–379.
[39] Y. Chu, X. Gao, X. Zhang, G. Xu, G. Li, A. Zheng, Identifying the effective phosphorous species over modified P-ZSM-5 zeolite: a theoretical study, PCCP 20 (2018) 11702–11712.
[40] S. Tian, S. Ji, D. Lü, B. Bai, Q. Sun, Preparation of modified Ce-SAPO-34 catalysts and their catalytic performances of methanol to olefins, J. Enegy Chem. 22 (2013) 605–609.
[41] N. Hadi, A. Niaei, S.R. Nabavi, M. Navaei Shirazi, R. Alizadeh, Effect of second metal on the selectivity of Mn/H-ZSM-5 catalyst in methanol to propylene process, J. Ind. Eng. Chem. 29 (2015) 52–62.
[42] T.-S. Zhao, T. Takemoto, N. Tsubaki, Direct synthesis of propylene and light olefins from dimethyl ether catalyzed by modified H-ZSM-5, Catal. Commun. 7 (2006) 647–650.
[43] Z. Song, A. Takahashi, N. Mimura, T. Fujitani, Production of propylene from ethanol over ZSM-5 zeolites, Catal. Lett. 131 (2009) 364–369.
[44] A.Z. Varzaneh, J. Towfighi, S. Sahebdelfar, Carbon nanotube templated synthesis of metal containing hierarchical SAPO-34 catalysts: IMPACT of the preparation method and metal avidities in the MTO reaction, Micropor. Mesopor. Mater. 236 (2016) 1–12.
[45] Y. Zhang, Y. Zhao, T. Otroshchenko, S. Han, H. Lund, U. Rodemerck, D. Linke, H. Jiao, G. Jiang, E.V. Kondratenko, The effect of phase composition and crystallite size on activity and selectivity of ZrO2 in non-oxidative propane dehydrogenation, J. Catal. 371 (2019) 313–324.
[46] Y. Zhang, Y. Zhao, T. Otroshchenko, H. Lund, M.-M. Pohl, U. Rodemerck, D. Linke, H. Jiao, G. Jiang, E.V. Kondratenko, Control of coordinatively unsaturated Zr sites in ZrO2 for efficient C–H bond activation, Nat. Commun. 9 (2018) 3794.
[47] C.-M. Wang, Y.-D. Wang, Z.-K. Xie, Verification of the dual cycle mechanism for methanol-to-olefin conversion in HSAPO-34: a methylbenzene-based cycle from DFT calculations, Catal. Sci. Technol. 4 (2014) 2631–2638.
[48] Y. Jeanvoine, J.G. Ángyán, G. Kresse, J. Hafner, Brønsted acid sites in HSAPO-34 and chabazite: an ab initio structural study, J. Phys. Chem. B 102 (1998) 5573–5580.
[49] C.-M. Wang, R.Y. Brogaard, B.M. Weckhuysen, J.K. Nørskov, F. Studt, Reactivity descriptor in solid acid catalysis: predicting turnover frequencies for propene methylation in zeotypes, J. Phys. Chem. Lett. 5 (2014) 1516–1521.
[50] D. Zhai, Y. Liu, H. Zheng, L. Zhao, J. Gao, C. Xu, B. Shen, A first-principles evaluation of the stability, accessibility, and strength of Brønsted acid sites in zeolites, J. Catal. 352 (2017) 627–637.
[51] B. Xing, J. Ma, R. Li, H. Jiao, Location, distribution and acidity of Al substitution in ZSM-5 with different Si/Al ratios - a periodic DFT computation, Catal. Sci. Technol. 7 (2017) 5694–5708.
[52] S. Shetty, B.S. Kulkarni, D.G. Kanhere, A. Goursot, S. Pal, A comparative study of structural, acidic and hydrophilic properties of Sn−BEA with Ti−BEA using periodic density functional theory, J. Phys. Chem. B 112 (2008) 2573–2579.
[53] A. Damin, S. Bordiga, A. Zecchina, K. Doll, C. Lamberti, Ti-chabazite as a model system of Ti(IV) in Ti-zeolites: a periodic approach, J. Chem. Phys. 118 (2003) 10183–10194.
[54] J.P. Perdew, K. Burke, M. Ernzerhof, Generalized gradient approximation made simple, Phys. Rev. Lett. 77 (1996) 3865–3868.
[55] G. Kresse, J. Hafner, Ab initio molecular dynamics for open-shell transition metals, Phys. Rev. B 48 (1993) 13115–13118.
[56] G. Kresse, J. Hafner, Ab initio molecular-dynamics simulation of the liquid-metal–amorphous-semiconductor transition in germanium, Phys. Rev. B 49 (1994) 14251–14269.
[57] G. Kresse, J. Furthmüller, Efficiency of ab-initio total energy calculations for metals and semiconductors using a plane-wave basis set, Comput. Mater. Sci. 6 (1996) 15–50.
[58] G. Kresse, J. Furthmüller, Efficient iterative schemes for ab initio total-energy calculations using a plane-wave basis set, Phys. Rev. B 54 (1996) 11169–11186.
[59] G. Kresse, D. Joubert, From ultrasoft pseudopotentials to the projector augmented-wave method, Phys. Rev. B 59 (1999) 1758–1775.
[60] P.E. Blöchl, Projector augmented-wave method, Phys. Rev. B 50 (1994) 17953–17979.
[61] H.J. Monkhorst, J.D. Pack, Special points for Brillouin-zone integrations, Phys. Rev. B 13 (1976) 5188–5192.
[62] S. Grimme, Semiempirical GGA-type density functional constructed with a long-range dispersion correction, J. Comput. Chem. 27 (2006) 1787–1799.
[63] G. Henkelman, B.P. Uberuaga, H. Jónsson, A climbing image nudged elastic band method for finding saddle points and minimum energy paths, J. Chem. Phys. 113 (2000) 9901–9904.
[64] Y. Chu, B. Han, H. Fang, A. Zheng, F. Deng, Influence of acid strength on the reactivity of alkane activation on solid acid catalysts: a theoretical calculation study, Micropor. Mesopor. Mater. 151 (2012) 241–249.
[65] L. Kang, T. Zhang, Z. Liu, K.-L. Han, Methanol adsorption in isomorphously substituted AlPO-34 clusters and periodic density functional theory calculations, J. Phys. Chem. C 112 (2008) 5526–5532.
[66] A. Gamba, G. Tabacchi, E. Fois, TS-1 from first principles, J. Phys. Chem. A 113 (2009) 15006–15015.
[67] G. Yang, Y. Wang, D. Zhou, X. Liu, X. Han, X. Bao, Density functional theory calculations on various M/ZSM-5 zeolites: Interaction with probe molecule H2O and relative hydrothermal stability predicted by binding energies, J. Mol. Catal. A Chem. 237 (2005) 36–44.
[68] B.D. Montejo-Valencia, M.C. Curet-Arana, DFT study of the lewis acidities and relative hydrothermal stabilities of BEC and BEA zeolites substituted with Ti, Sn, and Ge, J. Phys. Chem. C 119 (2015) 4148–4157.
[69] A.J. Jones, E. Iglesia, The strength of Brønsted acid sites in microporous aluminosilicates, ACS Catal. 5 (2015) 5741–5755.
[70] E. Aghaei, M. Haghighi, Z. Pazhohniya, S. Aghamohammadi, One-pot hydrothermal synthesis of nanostructured ZrAPSO-34 powder: effect of Zr-loading on physicochemical properties and catalytic performance in conversion of methanol to ethylene and propylene, Micropor. Mesopor. Mater. 226 (2016) 331–343.
[71] U. Olsbye, S. Svelle, M. Bjørgen, P. Beato, T.V.W. Janssens, F. Joensen, S. Bordiga, K.P. Lillerud, Conversion of methanol to hydrocarbons: how zeolite cavity and pore size controls product selectivity, Angew. Chem. Int. Ed. 51 (2012) 5810–5831.
[72] M. Seiler, W. Wei, A. Buchholz, M. Hunger, Direct evidence for a catalytically active role of the hydrocarbon pool formed on Zeolite H-ZSM-5 during the methanol-to-olefin conversion, Catal. Lett. 88 (2003) 187–191.
[73] B. Arstad, J.B. Nicholas, J.F. Haw, Theoretical study of the methylbenzene side-chain hydrocarbon pool mechanism in methanol to olefin catalysis, J. Am. Chem. Soc. 126 (2004) 2991–3001.
[74] D. Lesthaeghe, J. Van der Mynsbrugge, M. Vandichel, M. Waroquier, V. Van Speybroeck, Full theoretical cycle for both ethene and propene formation during methanol-to-olefin conversion in H-ZSM-5, ChemCatChem 3 (2011) 208–212.
[75] Y. Chu, B. Han, A. Zheng, F. Deng, Influence of acid strength and confinement effect on the ethylene dimerization reaction over solid acid catalysts: a theoretical calculation study, J. Phys. Chem. C 116 (2012) 12687–12695.
[76] Y. Chu, P. Ji, X. Yi, S. Li, P. Wu, A. Zheng, F. Deng, Strong or weak acid, which is more efficient for Beckmann rearrangement reaction over solid acid catalysts? Catal. Sci. Technol. 5 (2015) 3675–3681.
[77] Y. Chu, X. Sun, X. Yi, L. Ding, A. Zheng, F. Deng, Slight channel difference influences the reaction pathway of methanol-to-olefins conversion over acidic H-ZSM-22 and H-ZSM-12 zeolites, Catal. Sci. Technol. 5 (2015) 3507–3517.
[78] S. Kozuch, S. Shaik, How to conceptualize catalytic cycles? The energetic span model, Acc. Chem. Res. 44 (2011) 101–110.
[79] W. Zhang, J. Chen, S. Xu, Y. Chu, Y. Wei, Y. Zhi, J. Huang, A. Zheng, X. Wu, X. Meng, F. Xiao, F. Deng, Z. Liu, Methanol to olefins reaction over cavity-type zeolite: cavity controls the critical intermediates and product selectivity, ACS Catal. 8 (2018) 10950–10963.
[80] D.Y. Curtin, Stereochemical control of organic reactions differences in behavior of diastereomers, Rec. Chem. Prog. 15 (1954) 111–128.
[81] Z.-X. Yu, P.H.-Y. Cheong, P. Liu, C.Y. Legault, P.A. Wender, K.N. Houk, Origins of differences in reactivities of alkenes, alkynes, and allenes in [Rh(CO)2Cl]2-Catalyzed (5 + 2) cycloaddition reactions with vinylcyclopropanes, J. Am. Chem. Soc. 130 (2008) 2378–2379.
[82] S. Tobisch, Is an M-N σ-bond insertion route a viable alternative to the M=N [2+2] cycloaddition route in intramolecular aminoallene hydroamination/cyclisation catalysed by neutral zirconium Bis(amido) complexes? A computational mechanistic study, Chem. Eur. J. 14 (2010) 8590–8602.
[83] A.T. Normand, K.J. Hawkes, N.D. Clement, K.J. Cavell, B.F. Yates, Atom-efficient catalytic coupling of imidazolium salts with ethylene involving Ni−NHC complexes as intermediates: a combined experimental and DFT study, Organometallics 26

(2007) 5352–5363.
[84] K.J. Hawkes, K.J. Cavell, B.F. Yates, Rhodium-catalyzed C-C coupling reactions: mechanistic considerations, Organometallics 27 (2008) 4758–4771.
[85] A.E. Guiducci, C.L. Boyd, E. Clot, P. Mountford, Reactions of cyclopentadienyl-amidinate titanium imido compounds with CO2: cycloaddition-extrusion vs. cycloaddition-insertion, Dalton Trans. (30) (2009) 5960–5979.
[86] P. Liu, P.H.-Y. Cheong, Z.-X. Yu, P.A. Wender, K.N. Houk, Substituent effects, reactant preorganization, and ligand exchange control the reactivity in RhI-catalyzed (5 + 2) cycloadditions between vinylcyclopropanes and alkynes, Angew. Chem. Int. Ed. 47 (2008) 3939–3941.
[87] F. Bleken, M. Bjørgen, L. Palumbo, S. Bordiga, S. Svelle, K.P. Lillerud, U. Olsbye, The effect of acid strength on the conversion of methanol to olefins over acidic microporous catalysts with the CHA topology, Top. Catal. 52 (2009) 218–228.
[88] S. Xu, Y. Zhi, J. Han, W. Zhang, X. Wu, T. Sun, Y. Wei, Z. Liu, Chapter two - advances in catalysis for methanol-to-olefins conversion, in: C. Song (Ed.), Advances in Catalysis, Academic Press, 2017, pp. 37–122.